JACS
JOURNAL OF THE AMERICAN CHEMICAL SOCIETY

Article

pubs.acs.org/JACS

Optical Activity and Optical Anisotropy in Photomechanical Crystals of Chiral Salicylidenephenylethylamines

Akifumi Takanabe,[†] Masahito Tanaka,[‡] Kohei Johmoto,[§] Hidehiro Uekusa,[§] Tadashi Mori,[∥] Hideko Koshima,*[,⊥] and Toru Asahi*[,†,⊥]

[†]Department of Advanced Science and Engineering, Graduate School of Advanced Science and Engineering, Waseda University, 3-4-1 Okubo, Shinjuku-ku, Tokyo 169-8555, Japan

[‡]Research Institute for Measurement and Analytical Instrumentation, National Institute of Advanced Industrial Science and Technology (AIST), Tsukuba Central 2, 1-1-1 Umezono, Tsukuba, Ibaraki 305-8568, Japan

[§]Department of Chemistry and Materials Science, Graduate School of Science and Engineering, Tokyo Institute of Technology, 2-12-1 Ookayama, Meguro-ku, Tokyo 152-8551, Japan

[∥]Department of Applied Chemistry, Graduate School of Engineering, Osaka University, 2-1 Yamada-oka, Suita, Osaka 565-0871, Japan

[⊥]Researh Organization for Nano & Life Innovation, Waseda University, 513 Wasedatsurumaki-cho, Shinjuku-ku, Tokyo 162-0041, Japan

Supporting Information

ABSTRACT: Introducing chirality into photomechanical crystals is beneficial for the diversification of mechanical motion. Measurement of the chiroptical and optical anisotropic properties of chiral crystals is indispensable for evaluating photomechanical crystals. The platelike crystals of *S*- and *R*-enantiomers of photochromic *N*-3,5-di-*tert*-butylsalicylidene-1-phenylethylamine in enol form (enol-(*S*)-**1** and enol-(*R*)-**1**) caused bending motion with twisting upon ultraviolet (UV) light irradiation, due to shrinkage along the length and width directions of the irradiated surface, based on the optimized crystal structure of the photoisomerized *trans*-keto-(*S*)-**1**. By employing the generalized high-accuracy universal polarimeter (G-HAUP), optical anisotropic (linear birefringence, LB; linear dichroism, LD) as well as chiroptical (circular birefringence, CB; circular dichroism, CD) spectra of both the enantiomeric crystals on the (001) face were simultaneously measured before and under continuous UV irradiation. The LD peak was observed at 330 nm in the negative sign, derived from the $\pi-\pi^*$ transition of the intramolecularly hydrogen-bonded salicylidenimino moiety. The CD spectra of the *S* and *R* crystals revealed the negative and positive Cotton effect at 330 nm, respectively, and new peaks appeared at 460 nm under UV light irradiation due to photoisomerization to the *S* and *R* *trans*-keto isomers at around 10% conversion. The CB and CD spectra evaluated by the HAUP measurement were opposite to those measured in the hexane solution, as well as those simulated by quantum chemical calculation. The dissymmetry parameter, *g*, of the enol-(*S*)-**1** crystal along the *c* axis (0.013) was approximately 10 times larger than the *g* values in the solution (0.0010) and by calculation (0.0016).

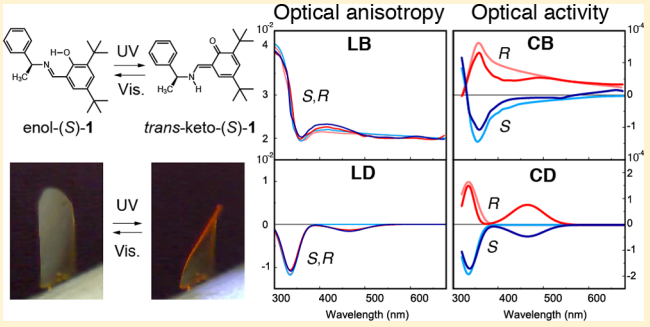

INTRODUCTION

Molecular machines based on the linkage of microscopic molecular motion to macroscale crystal motion have received substantial attention in the contexts of both basic research and their wide range of potential applications. Photomechanical motion involves the direct conversion of light energy to mechanical energy, which is beneficial in regard to energy conversion. Such mechanical crystals are amenable to remote operation with light and do not require wire connections. For example, Irie et al. reported reversible photomechanical bending in rod-shaped diarylethene crystals, successfully linking molecular-level shape changes to macroscale mechanical motion in crystals.[1] Similarly, Bardeen et al. demonstrated irreversible and reversible shape changes in rod-shaped anthracene nanocrystals.[2] Since then, increasing numbers of studies on the photomechanical motion of crystals, broadening to examine various photomechanical crystals such as diarylethenes,[3−5] anthracenes,[6−8] azobenzenes,[9,10] furylfulgides,[11] salicylideneanilines,[12] 4-chlorocinnamic acid,[13] benzylidenedimethylimidazolinone,[14] 1,2-bis(4-pyridyl)ethylene salt,[15] and naphthalene diimides,[16] have been reported in the past decade. Recently, reviews[17−20] and a book[21] on photomechanical crystals have also been published. Nevertheless, there is a need

Received: September 14, 2016
Published: October 24, 2016

DOI: 10.1021/jacs.6b09633
J. Am. Chem. Soc. 2016, 138, 15066−15077

for further development of new mechanical crystals with various characteristics to fulfill their wide application potential as synthetic molecular machinery.[22]

Solid-state photoreactivities in chiral crystals usually differ from those in achiral crystals because the motion of molecules is restricted in the crystal lattice, and the chiral environment is retained during reactions.[23] Photoinduced twisting motions of chiral diarylethene crystals in a left- and right-handed helical manner have been reported.[5b] We demonstrated that the chiral crystals of azobenzene derivatives exhibited photomechanical bending with twisting, while the racemic crystals bent very slightly without twisting, showing that the photomechanical behavior of chiral crystals was different from that of racemic crystals.[24] Despite the fact that platelike chiral crystals of salicylidenephenylethylamines [enol-(*S*)-**1** and enol-(*R*)-**1**] (Scheme 1) exhibited photomechanical bending similar to

Scheme 1. Photoinduced Hydrogen Transfer Reaction of Salicylidenephenylethylamines Enol-(*S*)-1 and Enol-(*R*)-1

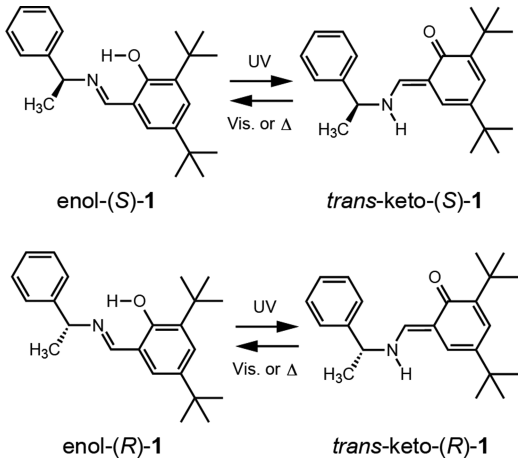

that of the racemic crystals [enol-(*rac*)-**1**], the durability of repeated bending and physical properties, such as Young's modulus and stress, were different between the chiral and racemic crystals: The Young's moduli are 0.76 GPa [enol-(*S*)-**1**] and 2.60 GPa [enol-(*rac*)-**1**], and the stress values are 0.68 MPa [enol-(*S*)-**1**] and 1.81 MPa [enol-(*rac*)-**1**].[25] The introduction of chirality is beneficial to increase diversification in photomechanical crystals.

Every chiral organic crystal has an inherent optical activity, exhibiting chiroptical properties of circular birefringence (CB) and circular dichroism (CD).[26] Moreover, many chiral and achiral crystals have optical anisotropy, such as linear birefringence (LB) and linear dichroism (LD). Measurement of the four optical properties of chiral crystals is necessary for evaluating photomechanical crystals. However, simultaneous measurement of CB, CD, LB, and LD is extremely difficult to conduct. The CB and CD signals are overwhelmed by the LB and LD signals because the latter are 10^2–10^3 times larger than the former.[27] Hence, conventional polarimeters and CD spectrophotometers cannot be applied to accurately measure CB and CD, except in one specific case, i.e., along the optic axis.

The high-accuracy universal polarimeter (HAUP) was developed in 1983[28] to measure the LB and CB of various crystals, such as glutamic acid[29] and chiral cocrystals.[30] The HAUP method has been extended to the measurement of anisotropic colored materials and has made possible the simultaneous measurement of LB and CB as well as LD and CD.[31] Recently, the HAUP apparatus was generalized using a conventional Xe lamp and a monochromator to obtain ultraviolet (UV) and visible region spectra (300–680 nm).[32] The generalized HAUP (G-HAUP) was then applied to intercalated $K_4Nb_6O_{17}$ crystals with an azobenzene derivative[32] and to laminated collagen membranes.[33]

We successfully measured the chiroptical (CB, CD) and optical anisotropic (LB, LD) spectra of the photomechanical crystals of both the enantiomeric salicylidenephenylethylamines enol-(*S*)-**1** and enol-(*R*)-**1** (Scheme 1) before and under UV light irradiation by the HAUP method. This is the first report of changes in the chiroptical and optical anisotropic properties accompanied by the reaction in the chiral crystals. The mechanism of photomechanical bending with twisting motion of the crystals was elucidated based on the optimized crystal structure of the photoisomerized *trans*-keto-(*S*)-**1** by calculation. The correlation between the changes of four optical properties and the changes of the crystal structures is discussed.

RESULTS AND DISCUSSION

Crystal Structures and Photomechanical Bending with Twisting Motion. The compounds enol-(*S*)-**1** and enol-(*R*)-**1** were synthesized as previously reported.[34] The crystal structure of enol-(*S*)-**1** was already determined, but that of *trans*-keto-(*S*)-**1** was not yet successfully determined.[25] Hence, *in situ* crystallographic analyses were carefully performed under continuous UV irradiation to analyze the crystal structure of *trans*-keto-(*S*)-**1**. Because no disorder was found in the crystals, we calculated the crystal structure of *trans*-keto-(*S*)-**1** by density functional theory (DFT-D) calculation (Figure 1b). The optimized crystal structure of enol-(*S*)-**1** using DFT-D (Figure 1a) belongs to the same space group ($P2_12_12_1$) and has similar geometrical features to the observed structure, in which intramolecular hydrogen bonds formed between the N atom of the C═N Schiff base and the H atom of the 2-OH

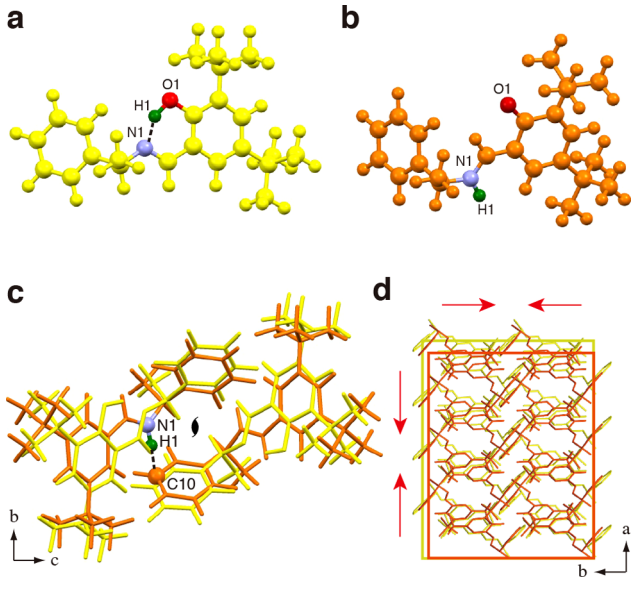

Figure 1. Crystal structures determined from DFT-D calculations: ball and stick drawings of (a) enol-(*S*)-**1** (yellow) and (b) *trans*-keto-(*S*)-**1** (orange). Overlaid molecular arrangements on (c) (100) face and (d) (00$\bar{1}$) face. The red arrows in d indicate the directions of the shrinkage of the *trans*-keto-(*S*)-**1** crystal along the *a* and *b* axes.

DOI: 10.1021/jacs.6b09633
J. Am. Chem. Soc. 2016, 138, 15066–15077

group of the salicylaldehyde ring; the N···O distance and N···H−O angle are 1.541 Å and 152.82°, respectively.

Comparing the calculated crystal structure of enol-(*S*)-**1** with that of *trans*-keto-(*S*)-**1**, changes in the unit cell dimensions were observed as shown in Table 1. The length of the *a* and *b* axes of the *trans*-keto-(*S*)-**1** unit cell decreased slightly (−3.70 and −3.32%, respectively), and the length of the *c* axis increased (+0.16%), supporting the cell deformation tendency after UV irradiation reported in the previous study.[25] Moreover, due to the slight shift of molecular position in the *trans*-keto-(*S*)-**1** crystals, we observed an N1···C10 distance of 3.262 Å and a N1−H···C10 angle of 141.9°, indicating the formation of N−H···π interaction (Figure 1c). Therefore, the *a* and *b* axes contracted, and the *c* axis extended.

Table 1. Unit Cell Sizes of Enol-(*S*)-1 and *trans*-Keto-(*S*)-1 Crystals Obtained from DFT-D Calculation

	enol-(*S*)-**1**	*trans*-keto-(*S*)-**1**	relative change (%)
a (Å)	6.0803	5.8555	−3.70
b (Å)	9.6333	9.3134	−3.32
c (Å)	35.4535	35.5093	+0.16
V (Å^3)	2076.6304	1936.4860	−6.75

Although we previously reported photomechanical bending of the platelike crystals of enol-(*S*)-**1**, a wide and thin platelike microcrystal (354 μm long ×87 μm wide ×10 μm thick) prepared by slow sublimation was submitted for the observation of photomechanical motion. Figure 2a shows the frontal (00$\bar{1}$) face with the longitudinal direction along the *a* axis, of which the lower portion was fixed to the needle with an adhesive and the upper portion was free. The relationship between the crystal faces and the wide surfaces of both enantiomeric enol-**1** crystals was determined using single-crystal X-ray structure analysis (Figure S1). When the (00$\bar{1}$) face was irradiated from the front at 365 nm with a UV-LED illuminator (50 mW cm^{-2}), the crystal bent toward the light source with slight left-handed twisting, reaching maximum deflection after 5 s (Figure 2b and Movie S1). Subsequent illumination with a pseudowhite LED lamp (broad bands at 465 and 560 nm) returned the bend and twist to the initial flat shape after 30 s. Irradiation of the (001) surface from the rear induced forward bending with a slight right-handed twist (Figure 2c and Movie S2). We already reported the repeatability of bending motion; alternating irradiation of the (001) face with UV and visible light caused a gradual decrease of the tip displacement angle (−15%) after 100 cycles.[25]

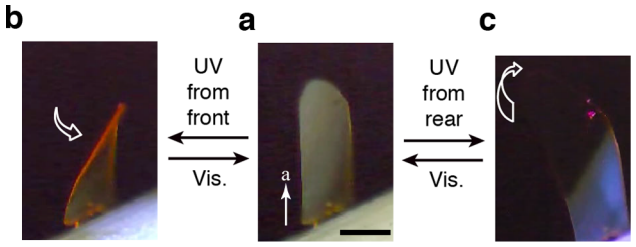

Figure 2. Bending with twisting motion of a wide and thin platelike microcrystal of enol-(*S*)-**1** (a) before UV light irradiation and after irradiation from (b) the front and (c) the rear. The scale bar is 100 μm.

We briefly explored a possible mechanism of the bending and twisting motion. An overlay of the molecular arrangements of the enol-(*S*)-**1** (yellow) and the *trans*-keto-(*S*)-**1** (orange) is shown in Figure 1d. On the (00$\bar{1}$) face, the molecules of enol-(*S*)-**1** are arranged in a 2-fold helical manner along the *a* axis to form a columnar structure. Upon UV irradiation of the (00$\bar{1}$) face, both the length and width along the *a* and *b* axes shrank near the front crystal surface due to photoisomerization to the *trans*-keto-(*S*)-**1** molecules. The contraction is considered to occur in the diagonal direction. In contrast, the length and width do not change at the back surface of the crystal, due to a lack of penetration of the irradiated light and no occurrence of photoisomerization. Hence, the thin and wide platelike crystal bends toward the light source with a twisting motion in a right-handed helix (Figure 3a). Conversely, UV irradiation of the (001) face causes bending with twisting in a left-handed helix (Figure 3b).

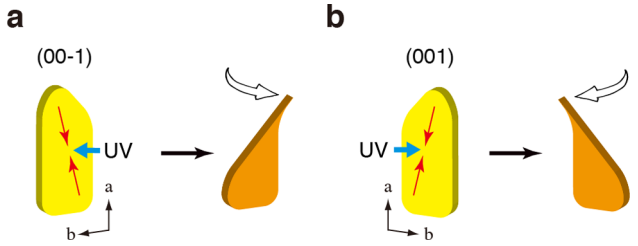

Figure 3. Relationship between the direction of twisting and the face of enol-(*S*)-**1** crystal irradiated with UV light: (a) twist in right-handed helix; (b) twist in left-handed helix. The red arrows indicate the directions of the shrinkage of the enol-(*S*)-**1** crystal along the diagonal of the *a* and *b* axes.

Chiroptical and Optical Anisotropic Properties. Thin and wide platelike enol-(*S*)-**1** and enol-(*R*)-**1** crystals with smooth surfaces are required for HAUP measurement, due to the transmission optical system of the apparatus (Figure S2). Most thin specimens are prepared by polishing single crystals. However, it was extremely difficult to decrease the thickness of the single enol-(*S*)-**1** crystals grown by recrystallization to less than a few tens of micrometers by polishing with lapping films. Furthermore, the polishing scratches remained even when using lapping film coated with a soft Fe_2O_3 polishing agent with very fine particles (0.3 μm). The specimen preparation problem was overcome by applying the sublimation method. The enol-(*S*)-**1** powders were put in a 30 mL glass beaker, and a few glass plates were placed against its inside wall. Then, the beaker was covered and heated at 80 °C for several weeks. After much trial and error, we used this gentle sublimation method to obtain very thin and wide platelike single enol-(*S*)-**1** crystals, whose thickness was less than 10 μm and length and width were approximately 3 and 1 mm, respectively (Figure 4a). The (001) top surface was sufficiently smooth and suitable for HAUP measurement. Similarly, we obtained thin, platelike crystals of enol-(*R*)-**1** by this sublimation method. Using silicone grease, the thin crystal was fixed on a thin Cu plate with a 0.5 mm diameter pinhole for the light beam to pass through (Figure 4b).

Linearly polarized UV−vis absorption spectra of enol-(*S*)-**1** crystal, before and under continuous UV irradiation, were measured using the HAUP with the analyzer removed. The polarized light was incident perpendicularly on the (001) top surface of the thin (10 μm) crystal and transmitted parallel to

DOI: 10.1021/jacs.6b09633
J. Am. Chem. Soc. 2016, 138, 15066−15077

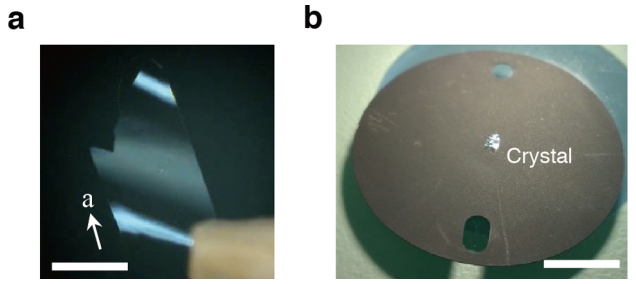

Figure 4. (a) Photograph of a thin platelike crystal of enol-(*S*)-**1** obtained by sublimation. The scale bar is 500 μm. (b) Crystal fixed on a Cu sample plate with a pinhole of 0.5 mm in diameter. The scale bar is 10 mm.

the *c* axis. UV-LED light (365 nm) was continuously irradiated at low power (10 mW cm^{-2}) from a direction almost vertical to the HAUP light path, to prevent incidence to the photomultiplier tube (see detail in Figure S5). Bending of the crystal by the UV irradiation was prevented by fixing the crystals to the Cu plate (thickness: 0.12 mm) with silicone grease.

Before UV irradiation, a strong absorption peak at 330 nm was observed, which was derived from the $\pi-\pi^*$ transition of the intramolecular hydrogen-bonded salicylidenimino moiety (Figure 5a).[35,36] The peak heights decreased as the vibration direction was changed from parallel (0°) to perpendicular (90°) to the *a* axis, showing the anisotropic character of the crystal. Under UV irradiation, a new absorption peak at 460 nm appeared due to the formation of *trans*-keto-(*S*)-**1** by photochemical hydrogen transfer reaction (Figure 5b), consistent with the previous study.[25,37] This absorption peak affects the crystal color from pale yellow to reddish-orange. Both absorption bands at 330 and 460 nm yielded maxima (peak heights) at the parallel (0°) vibration direction of the linearly polarized light to the *a* axis. Both peak heights decreased as the vibration direction changed from parallel (0°) to perpendicular (90°) to the *a* axis.

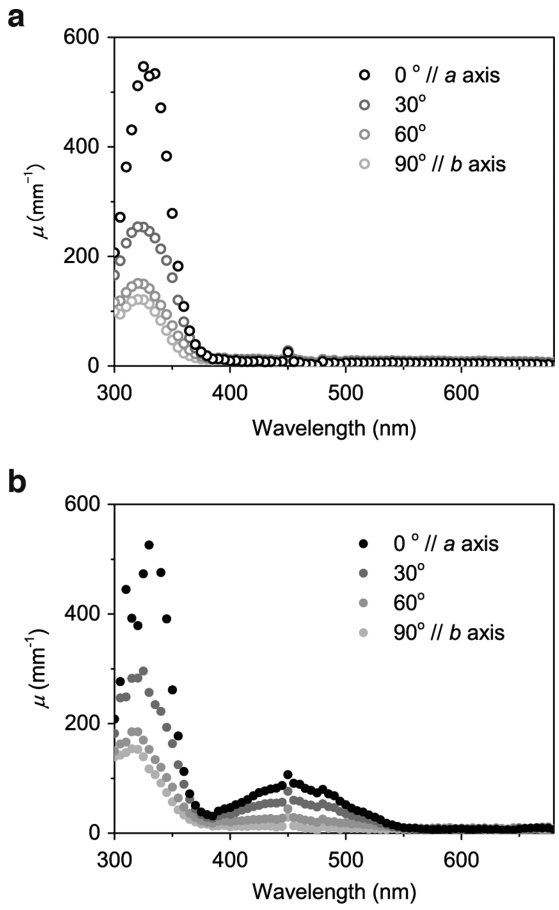

Figure 5. Linearly polarized UV−vis absorption spectra of enol-(*S*)-**1** crystal on the (001) face (a) before and (b) under continuous UV light irradiation at 365 nm. The value of μ expresses absorption coefficient. The vibration directions of incident linearly polarized light were changed from parallel to perpendicular to the *a* axis.

We adopted the HAUP method[32] to simultaneously measure all optical anisotropic (LB, LD) and chiroptical (CB, CD) spectra of both the enol-(*S*)-**1** and enol-(*R*)-**1** crystals, before and under continuous UV irradiation. The basis of the HAUP method is to measure the intensities of emergent light passing through a polarizer, crystal sample, and then analyzer as the azimuth angles of the polarizer and analyzer are independently altered. The HAUP method is described in detail in the Supporting Information. The G-HAUP apparatus is shown in Figure S2. Measurements were performed in the wavelength region between 300 and 680 nm at 293 K. The thicknesses of the thin, platelike crystals of enol-(*S*)-**1** and enol-(*R*)-**1** were 6.5 and 7.6 μm, respectively.

Figure 6 shows the LB, LD, CB, and CD spectra of the enol-(*S*)-**1** and enol-(*R*)-**1** crystals on the (001) face before UV irradiation. Optical properties of enol-(*R*)-**1** crystal in the wavelength range of 340−365 nm could not be measured as understood from Figure 6, because the value of recorded phase differences in this wavelength region belong to the inaccurate region for the HAUP measurement ($0.9\pi < \Delta_r \leq \pi$, or cos Δ_r almost equal to −1). The LB and LD spectra between the *S* and *R* enantiomeric crystals are coincident (Figure 6a,b), because optical anisotropic properties are not related to the chirality of the crystals. The LD peak at 330 nm was observed to be negative, which corresponds to the $\pi-\pi^*$ transition of the intramolecularly hydrogen-bonded salicylidenimino moiety. The LB spectra exhibited anomalous dispersion of negative peaks at 360 nm with a change in sign at the strong LD peak. Consequently, these results show that the LB and LD spectra satisfy the Kramers−Kronig relationship,[38] as shown in Figure S6a.

The CD spectra of enol-(*S*)-**1** and enol-(*R*)-**1** crystals revealed, respectively, strong negative and positive Cotton effects at 330 nm which mirror each other (Figure 6d). The CB spectrum of enol-(*S*)-**1** crystals also exhibited anomalous dispersion of negative peaks at 360 nm with changes in sign at the CD peaks, as in the case of LB and LD spectra (Figure 6c). Although the data plots of enol-(*R*)-**1** in the wavelength range of 340 to 365 nm could not be measured, the CB spectrum of enol-(*R*)-**1** is considered to exhibit anomalous dispersions of positive peak at around 360 nm because the CB spectra of enol-(*S*)-**1** and enol-(*R*)-**1** crystals should mirror each other. The baseline is slightly shifted to the positive in the CB spectra, which we consider to be caused by the inaccuracy of systematic error evaluations. The Kramers−Kronig relationship also holds between the CB and CD spectra (Figure S6c). It is reasonable that the magnitudes of the CB and CD are approximately 10^{-4}, smaller by two orders than the 10^{-2} of the LB and LD. These consistent results indicate that the CB and CD spectra were successfully obtained by the HAUP method.

DOI: 10.1021/jacs.6b09633
J. Am. Chem. Soc. 2016, 138, 15066−15077

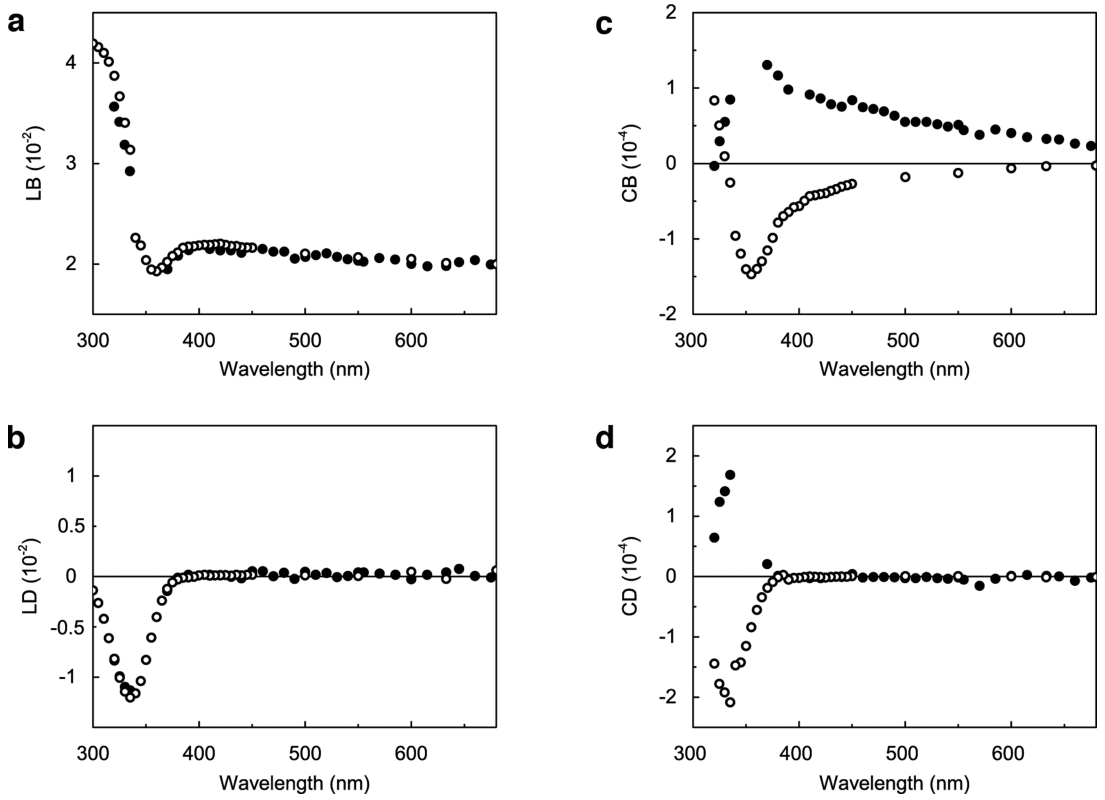

Figure 6. Anisotropic optical and chiroptical spectra of enol-(*S*)-**1** (black open circle) and enol-(*R*)-**1** (black solid circle) crystals on the (001) face at 293 K: (a) LB, (b) LD, (c) CB, and (d) CD.

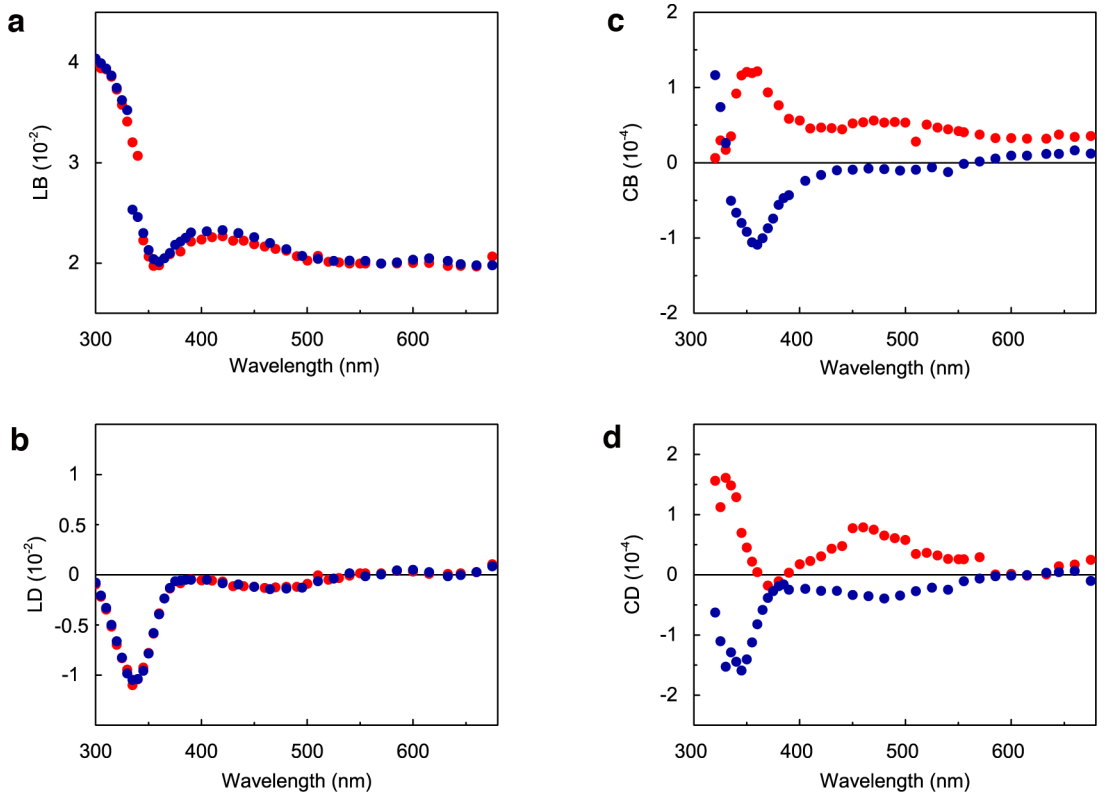

Figure 7. Anisotropic optical and chiroptical spectra of enol-(*S*)-**1** (dark blue solid circle) and enol-(*R*)-**1** (red solid circle) crystals on the (001) face under continuous UV light irradiation at 365 nm: (a) LB, (b) LD, (c) CB, and (d) CD.

We then attempted to measure the LB, LD, CB, and CD spectra of both enantiomeric enol-**1** crystals under UV irradiation. UV-LED light (365 nm) was continuously irradiated from a direction almost vertical to the HAUP light

DOI: 10.1021/jacs.6b09633
J. Am. Chem. Soc. 2016, 138, 15066−15077

path at low power (5 mW cm^{-2}) to minimize incidence of the UV light to the photomultiplier tube (Figure S5). Crystal bending by UV irradiation was prevented by fixing the crystals to the Cu plate with silicone grease. Even under such weak UV irradiation, the thicknesses of the enol-(*S*)-**1** and enol-(*R*)-**1** crystals decreased from 6.2 to 5.4 μm (−0.8 μm, −12.9%) and from 7.1 to 6.3 μm (−0.8 μm, −11.3%), respectively, after the 3 days required for the HAUP measurement. To explain this decrease in thickness, we measured the surface temperature of the crystal specimens using infrared (IR) thermometers and found that the surface temperature was elevated by approximately 0.5 °C under UV irradiation (See data in Figures S7 and S8). These results suggest that the crystal thickness might decrease by gradual sublimation from the top surface of the specimens heated during the long measurement period, despite temperature control with a thermostat. Therefore, when we obtain LB, LD, CB, and CD from raw experimental data via HAUP measurement, we should take into account the decrease in thickness of the specimen by UV irradiation. The specimen thickness at each wavelength was corrected by dividing the total change in thickness by the number of HAUP measurements.

Figure 7 shows the LB, LD, CB, and CD spectra under continuous UV irradiation at 365 nm, which represents the spectra at the photostationary state of the reactant enol-**1** and the product *trans*-keto-**1**. New LD peaks corresponding to *trans*-keto-(*S*)-**1** and *trans*-keto-(*R*)-**1** appeared at around 460 nm, and the magnitudes of the LD peaks at 330 nm decreased slightly. The LD spectra of the *S* and *R* *trans*-keto isomers were coincident (Figure 7b). The LB spectra exhibited a slight anomalous dispersion of positive and negative peaks at around 410 and 360 nm with a change in sign at the weak LD peak (Figure 7a). The changes of LB and LD spectra before and under UV irradiation are shown in Figure S9a,b, respectively. These results confirm that the LB and LD spectra satisfy the Kramers−Kronig relationship (Figure S6b).

New small negative and positive CD peaks appeared at 460 nm due to the formation of *trans*-keto-(*S*)-**1** and *trans*-keto-(*R*)-**1** crystals, respectively, and the magnitudes of CD peaks at 330 nm decreased slightly (Figure 7d). The CB spectra also exhibited anomalous dispersions of negative [enol-(*S*)-**1**] and positive [enol-(*R*)-**1**] peaks at 500 and 360 nm with a change in sign at the new CD peak (Figure 7c), as with the LB and LD spectra. The baseline is shifted slightly with regard to the positive in the CB spectra, which we consider to be caused by the inaccuracy of systematic error evaluations. The Kramers−Kronig relationship also roughly holds between the CB and CD spectra (Figure S6d). As shown in Figures S9, the CD and CB spectra under weak UV light irradiation are also successfully measured by the HAUP method.

Optical Properties and Crystal Structures Relationship. The linearly polarized UV−vis absorption spectra of the enol-(*S*)-**1** crystal yielded a maximum peak height in the (0°) vibration direction parallel to the *a* axis and decreased as the vibration direction changed to yield the minimum absorption perpendicular (90°) to the *a* axis (Figure 5). The absorption spectra of analogous *N*-salicylideneaniline crystals in enol and *trans*-keto forms are related to the direction of the $\pi-\pi^*$ transition dipole moments.[39] We also calculated the directions of the $\pi-\pi^*$ transition dipole moments of the enol-(*S*)-**1** and *trans*-keto-(*S*)-**1** crystals, revealing that the directions of the electronic transition moment incline only 3.0 and 14°, respectively, from the *a* axis on the (001) plane, almost parallel to the *a* axis [Figure 8; see detailed calculation method in the Experimental Section and the highest occupied molecular orbital (HOMO) and lowest unoccupied molecular orbital (LUMO) in Figure S10]. Hence, strong absorptions are induced by linearly polarized light in the vibration direction parallel to the *a* axis on the (001) face of the enol-(*S*)-**1** without and with UV irradiation.

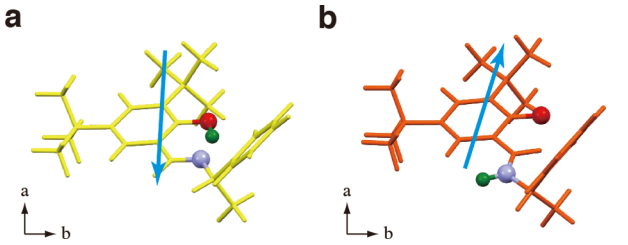

Figure 8. Directions of electronic transition dipole moment of (a) enol-(*S*)-**1** and (b) *trans*-keto-(*S*)-**1** on the (001) face in the crystals, shown as blue arrow.

We examined the correlation between the photomechanical motion of enol-(*S*)-**1** crystal and the polarization direction of irradiated UV light. The platelike crystal (4516 μm long × 380 μm wide × 97 μm thick) bent with right-handed twisting by irradiation with linearly polarized UV (365 nm) light almost parallel to the *a* axis (Figure S11b and Movie S3). Consequently, the irradiated surface was assigned to be the $(00\bar{1})$ face. In contrast, irradiation with polarized UV light perpendicular to the *a* axis scarcely caused crystal bending due to low absorption of the light (Figure S11c and Movie S4).

LD spectra were independently calculated from the linearly polarized UV−vis absorption spectra (Figure 5) by

$$\mathrm{LD} = \frac{\lambda}{4\pi d}[-\ln \Gamma_{\perp} - (-\ln \Gamma_{\parallel})] \quad (1)$$

where λ, d, and Γ are wavelength, sample thickness parallel to the direction of the incident light, and the ratio of intensity of transmitted light to intensity of incident light, respectively. The subscripts $\parallel$ and $\perp$ are the vibration directions of incident linearly polarized light parallel and perpendicular to the orientation axis, respectively.[40] For the enol-(*S*)-**1** crystal, $\parallel$ and $\perp$ corresponded to the *a* and *b* axes on the (001) plane, respectively. Figure 9 shows the calculated LD spectra of enol-

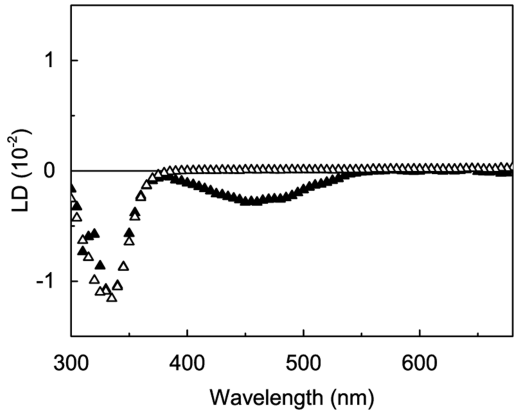

Figure 9. LD spectra of the enol-(*S*)-**1** crystal before (open triangle) and under continuous UV light irradiation (solid triangle) calculated from the linearly polarized absorption spectra in Figure 5.

DOI: 10.1021/jacs.6b09633
J. Am. Chem. Soc. 2016, 138, 15066−15077

Table 2. Linear Birefringences and Optical Rotatory Powers of Organic Crystals

crystal	λ (nm)	LB (10^{-2})	ρ (deg mm^{-1})	ref
(*S*)-salicylidenephenylethylamine	632.8	2.0	ρ_3 −5.2	this work
M-cocrystal: tryptamine/4-chlorobenzoic acid	632.8	18.5	ρ_1 +138	30
		21.1	ρ_2 −56	
		39.7	ρ_3 −355	
oxo amide	496.5	14.4	ρ_1 −79	41
		11.1	ρ_2 −32	
		3.4	ρ_3 −68	
L-glutamic acid	632.8	12.1	ρ_1 −31	29
		11.0	ρ_2 −98	
		0.9	ρ_3 +5.4	
L-aspartic acid	632.8	10.1	ρ_1 +223	42
		2.5	ρ_2 −19	
		12.7	ρ_3 −31	
Rochelle salt $NaKC_4H_4O_6{\cdot}4H_2O$	632.8	0.12	ρ_1 −1.0	43
lysozyme	488	0.24	ρ_1 −2.1	44
		0.24	ρ_3 +2.5	
azobenzene derivative intercalated into $K_4Nb_6O_{17}$	450	0.25	+0.1	32
laminated collagen membrane	300	0.88	−20	33

(*S*)-**1** crystal before and under continuous UV irradiation at 365 nm. The signs of both LD peaks at 330 and 460 nm were negative, which were coincident with those obtained by HAUP measurement (Figures 6b and 7b).

The conversion of photoisomerization of enol-(*S*)-**1** to *trans*-keto-(*S*)-**1** was calculated to be 18 ± 3.2% by comparison with the LD values fitted by Gaussian functions (Figure S12) at 330 nm, before and under continuous UV irradiation. On the other hand, the conversions of enol-(*S*)-**1** and enol-(*R*)-**1** crystals from the LD spectra by the HAUP measurement (Figures 6b and 7b) were calculated to be 10 ± 1.1% and 8.4 ± 3.4%, respectively. The smaller conversions are probably caused by the lower power (5 mW cm^{-2}) of the irradiated UV light in the HAUP measurement compared to that (10 mW cm^{-2}) in the measurement of the linearly polarized UV−vis absorption spectra (Figure 9). Normally, the photoisomerization should reach the photostationary state under continuous UV irradiation. Assuming that the photoisomerization reaction proceeded completely to produce the *trans*-keto-(*S*)-**1** at 100% yield, the magnitudes of the LD peaks at 460 nm are estimated to be -1.55×10^{-2} and -1.47×10^{-2} from the conversions (18 and 10%) of enol-(*S*)-**1** by the linearly polarized light absorption measurement (Figure S12) and the HAUP measurement (Figure S13b), respectively, which are very similar.

The LB of both enantiomeric enol-**1** crystals along the *c* axis showed a relatively lower value (0.02) above 600 nm than the previously reported organic crystals (Table 2). As shown in the packing diagrams (Figure 10a,b) the total intermolecular interaction in the enol-(*S*)-**1** crystal along all directions is the van der Waals force alone. This very weak molecular interaction may have induced such a small LB. In fact, we have reported a much larger value (0.4) for the LB of the chiral cocrystal composed of tryptamine and 4-chlorobenzoic acid (Table 2).[30] This cocrystal exhibits strong intermolecular interactions, such as the ionic bridging, hydrogen bonding, and the $\pi-\pi$ interaction of the aromatic moieties. Under UV irradiation, the weak N−H···π intermolecular interaction is formed in the *trans*-keto-(*S*)-**1** (Figure 1c). However, the total intermolecular interactions along the *c* axis appear to be weak because molecular packing in the *trans*-keto-(*S*)-**1** crystal (Figure 10c,d)

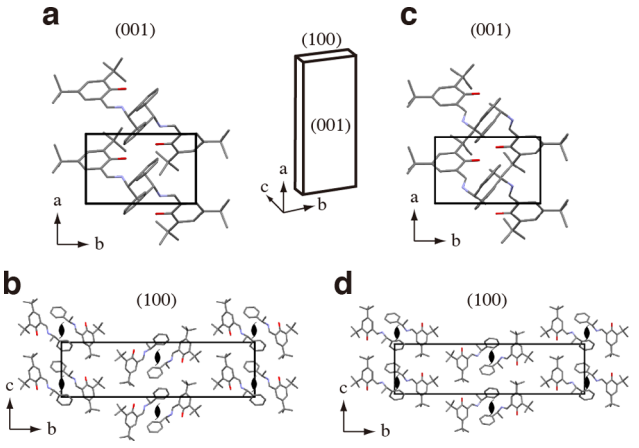

Figure 10. Molecular arrangements of (a and b) enol-(*S*)-**1** and (c and d) *trans*-keto-(*S*)-**1** crystals on (a and c) (001) and (b and d) (100) planes. Both crystal structures are obtained from the DFT-D calculation. All hydrogen atoms are omitted for clarity.

is similar to that of enol-(*S*)-**1** (Figure 10a,b). Hence, the differences in LB magnitudes above 600 nm of the enol-**1** crystals were small before and under continuous UV irradiation (Figure S13a,c).

Upon UV irradiation of the enol-(*S*)-**1** crystal, strain and stress are generated by changes in unit cell sizes due to photoisomerization to *trans*-keto-(*S*)-**1** near the crystal surface. We have previously reported the strain and stress values to be −0.31% and 0.68 MPa, respectively.[25] Despite the total prevention of bending motion by fixing the crystal to a thin Cu plate with silicon grease for the HAUP measurement, internal stress should arise even under weak UV irradiation (5 mW cm^{-2}); thereby, the observed LB (Figure 7a) might include the birefringence caused by stress. However, it is suggested that the stress birefringence along the *c* axis might be very small due to the high similarity between LB values above 600 nm before and under UV irradiation (Figure S9a).

In chemistry and biochemistry, specific optical rotation (α, degrees at 10 cm path length and *c* = 1.0 g per 100 cm^3) has been commonly used instead of CB as an expression of optical activity in solution. Hence, we would like to discuss here the

DOI: 10.1021/jacs.6b09633
J. Am. Chem. Soc. 2016, 138, 15066−15077

use of optical rotatory power (ORP)[32] (ρ, degree per 1 mm thickness). ORP is calculated as

$$\mathrm{ORP} = \frac{\pi}{\lambda}\mathrm{CB} \tag{2}$$

where λ is wavelength. ORP spectra of enol-(*S*)-**1** and enol-(*R*)-**1** crystals are shown in Figure 11a. The signs of ORP

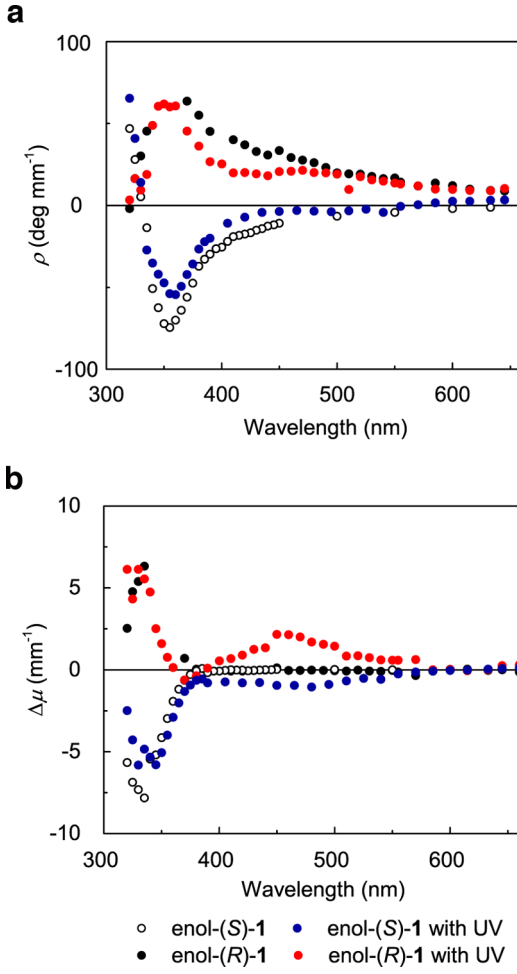

Figure 11. (a) ORP and (b) CD spectra of enol-(*S*)-**1** and enol-(*R*)-**1** crystals on the (001) face before and under continuous UV irradiation.

dispersion along the *c* axis are opposite to those in the hexane solution, which represent the signs averaged from every direction (Figure S14a). This suggests that the contribution from the ORP dispersion along the *c* axis might be small, or the ORP dispersions along the *a* and/or *b* axes might be largely positive in sign.

The ρ value of enol-(*S*)-**1** crystals along the *c* axis at 632.8 nm before UV irradiation was calculated to be −5.2° mm^{-1} after compensating the baseline by $(S - R)/2$, because the baseline of ORP spectra (Figure 11a) of enol-(*S*)-**1** and enol-(*R*)-**1** is shifted slightly to the positive. The μ value seems smaller than that in previous reports of organic crystals, as shown in Table 2. According to the HAUP theory, ORP and CB can be obtained from LB by

$$\mathrm{ORP} = \frac{\pi}{\lambda}\mathrm{CB} = \frac{2\pi}{\lambda}\mathrm{LB}k \tag{3}$$

where k is the ellipticity of eigen polarization. From eq 3, the magnitude of ORP is directly proportional to the magnitude of LB and k. Therefore, a small ORP should be induced by small LB and k values.

Molar CD, $\Delta\varepsilon$ (absorbance difference between right and left circularly polarized light at 1 M and 1 cm path length) has been commonly used as a unit of CD in solution. Herein we use $\Delta\mu$ (absorbance difference between right and left circularly polarized light per 1 mm thickness) as an expression of CD in a crystal. CD is calculated as

$$\mathrm{CD} = \frac{\lambda}{4\pi d}[-\ln \Gamma_l - (-\ln \Gamma_r)] \tag{4}$$

where the subscripts r and l are the incident right and left circular polarized light, respectively. Then, the $\Delta\mu$ can be calculated as

$$\Delta\mu = \frac{1}{d}[-\ln \Gamma_l - (-\ln \Gamma_r)] = \frac{4\pi}{\lambda}\mathrm{CD} \tag{5}$$

The $\Delta\mu$ spectra of enol-(*S*)-**1** and enol-(*R*)-**1** crystals are shown in Figure 11b. The signs of both CD ($\Delta\mu$) peaks at 330 nm are opposite to those in the hexane solution, as shown in Figure S14b.

The conversions of enol-(*S*)-**1** and enol-(*R*)-**1** to *trans*-keto-(*S*)-**1** and *trans*-keto-(*R*)-**1** were calculated to be 15 ± 3.9% and 13 ± 10%, respectively, by comparison with the CD spectra (Figure S9d) at 330 nm by the HAUP measurement, i.e., almost comparable. On the other hand, as mentioned above, the conversions of enol-(*S*)-**1** and enol-(*R*)-**1** calculated from the LD spectra (Figure S13b,d) by the HAUP measurement were 10% and 8.4%, respectively, showing different conversion values from the CD spectra. After the 3 days required for HAUP measurement, the sample thickness decreased due to gradual sublimation under UV light irradiation. The deterioration of the surface condition of the sample may have affected the accuracy of the HAUP measurement, especially in CD and CB due to the very small order of 10^{-4} (Figures 6c,d and 7c,d). Therefore, it might be desirable to adopt 10 and 8.4% as the conversions calculated from the LD spectra.

The CD and UV−vis spectra of isolated molecule **1** were simulated by the combined quantum chemical calculations. The geometries of enol-(*S*)-**1**, *cis*-keto-(*S*)-**1**, and *trans*-keto-(*S*)-**1** were optimized using the dispersion-corrected DFT method at the DFT-D3(BJ)-TPSS/def2-TZVP level.[45] The geometry thus obtained for the enol form was found to be generally consistent with that obtained by the X-ray crystallographic structure (Table S1).[25] The rotational strengths were then calculated by the time-dependent approximate coupled cluster method (RI-CC2/def2-TZVP).[46] The CD and UV−vis spectra were simulated by overlapping Gaussian functions for each transition, where the width of the band at 1/e height is fixed at 0.4 eV and the excitation energies were red-shifted by 0.3 eV (Figure 12).[47]

The calculated CD and UV−vis spectra for the enol-(*S*)-**1** reproduced the solution experiment results well (Figure S14). The calculated CD spectrum for *trans*-keto-(*S*)-**1** exhibits the positive Cotton effect at 460 nm, the same sign for enol-(*S*)-**1** at 330 nm. Conversely, *cis*-keto-(*S*)-**1** exhibits the negative Cotton effect at 440 nm. As the signs of Cotton effects of enol-(*S*)-**1** with UV irradiation at 330 and 460 nm obtained by the HAUP measurement are same, the Cotton effect of *cis*-keto-(*S*)-**1** might not contribute to the results obtained using HAUP with UV irradiation. This may be because the *cis*-keto form was

DOI: 10.1021/jacs.6b09633
J. Am. Chem. Soc. 2016, 138, 15066−15077

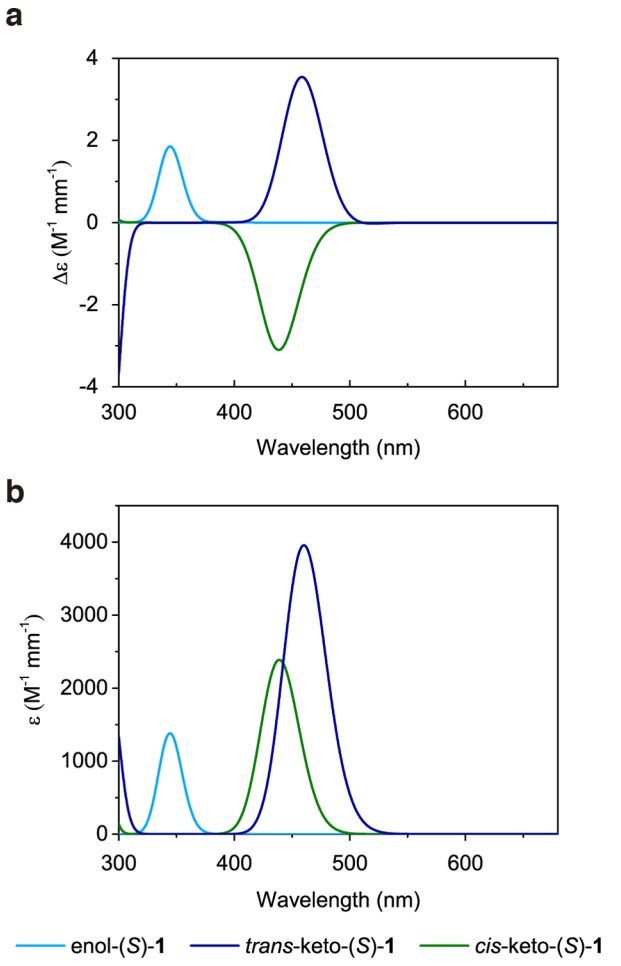

Figure 12. Calculated (a) CD and (b) UV−vis absorption spectra of (*S*)-**1** molecule.

not generated upon photoirradiation. This explanation is consistent with the previous report on photoisomerization of salicylideneaniline.[48]

Finally, we discuss the dissymmetry parameter, *g*, in the crystalline state, which is defined as the ratio in magnitude of $\Delta\mu$ to μ, i.e., $|\Delta\mu|/\mu$. The *g* value of enol-(*S*)-**1** crystal along the *c* axis was calculated to be 0.013 from the $|\Delta\mu|$ (6.9 mm^{-1}) of the negative CD peak at 330 nm (Figure S15b) and the μ (551 mm^{-1}) of the linearly polarized absorption peak parallel to the *a* axis at 330 nm (Figure 5a). On the other hand, the *g* value of enol-(*S*)-**1** in hexane solution was calculated to be 0.0010 from Figure S14a,b, and the *g* value from the calculated CD and absorption (Figure 12) was 0.0016, revealing that the *g* value of enol-(*S*)-**1** crystal obtained by the HAUP measurement without UV irradiation is around 10 times larger than *g* values in the solution and by the calculation. To our knowledge, this is the first report of a comparison of the *g* value of a single crystal along the crystal axis, not the optic axis, with that in solution and by calculation. For reference, the *g* value of L-alanine of the thin deposited film, not a single crystal, has been reported to be 0.0091 at 184 nm,[49] which is around 45 times larger than the *g* value in solution (0.0002).[50,51] In conclusion, the intramolecular and intermolecular interactions in crystalline state might enhance the dissymmetry parameter, *g*.

CONCLUSIONS

Optical anisotropic (LB and LD) and chiroptical (CB and CD) spectra of the chiral photomechanical crystals on the (001) face were simultaneously measured before and under continuous UV light irradiation by the G-HAUP. The platelike crystals of photochromic *S*- and *R*-salicylidenephenylethylamine in enol form caused bending motion with twisting upon UV irradiation, due to shrinkage along the length and width directions based on the optimized crystal structure of the photoisomerized *trans*-keto-isomer by calculation. The HAUP measurement was achieved by the careful preparation of thin (<10 μm) platelike crystals by gentle sublimation and by the prevention of crystal bending under UV irradiation by fixing the crystal to the sample plate with silicon grease. The CD spectra of the *S* and *R* crystals revealed a negative and positive Cotton effect at 330 nm, respectively, and new peaks appeared at 460 nm under UV light irradiation due to the photoisomerization to the *R* and *S* *trans*-keto isomers. The magnitudes of CB and CD were around 10^{-4}, i.e., smaller by two orders than those (around 10^{-2}) of LB and LD. The Kramers−Kronig relationship held between the LB and the LD, as well as the CB and the CD, before and under continuous UV irradiation. The CB and CD spectra obtained by the HAUP measurement were opposite to those measured in the hexane solution, as well as those simulated by quantum chemical calculation. The dissymmetry parameter (*g*) value of the crystal along the *c* axis was around 10 times larger than those in the solution and by calculation, showing that the dissymmetry parameter could be enhanced by intramolecular and intermolecular interactions in the crystals. In this study, the long measurement time caused a slight deterioration of crystal samples. Improvement of the G-HAUP apparatus is required to shorten the measurement time in future.

EXPERIMENTAL SECTION

Sample Preparation. Compounds enol-(*S*)-**1** and enol-(*R*)-**1** were synthesized according to a published protocol.[34] The melting points of enol-(*S*)-**1** (92−93 °C) and enol-(R)-**1** (92−93 °C) were identical. Thin, platelike single crystals of enol-(*S*)-**1** and enol-(*R*)-**1** were prepared by sublimation at 10−20 °C below the melting points. The top surface was assigned to be the (001) face in the longitudinal direction along the *a* axis, based on comparison with the platelike bulk single crystals obtained by recrystallization from solution. The thicknesses of all samples for the HAUP measurement were measured by laser microscopy (VK-X200; Keyence). Using silicone grease, the samples were fixed on a thin Cu plate with a pinhole of diameter 0.5 mm.

Crystal Structure Calculation. *trans-Keto-(S)-1.* The skeleton of the *trans*-keto-(*S*)-**1** molecule was constructed from enol-(*S*)-**1** molecule[25] by applying the pedal-motion phenomenon (Scheme 1).[52,53] There were two torsional angle degrees of freedom for the constructed *trans*-keto-(*S*)-**1** molecule around the phenylethyl moiety. The angles were determined to achieve the maximum overlap of molecules of *trans*-keto-(*S*)-**1** and enol-(*S*)-**1** molecules, i.e., phenyl rings occupy the same plane and methyl group situates at almost the same place (Figure 1c). Such maximum overlap structure of two topochemical isomer molecules has been observed in crystals of photochromic salicylideneamines,[53] in which two isomers occupy the same site, showing a disordered structure. The molecular arrangement (molecular packing and space group) was also taken from the enol-(*S*)-**1** crystal; thus, the presumed crystal structure of *trans*-keto-(*S*)-**1** was constructed.

This crystal structure was optimized by DFT-D calculations (PBE exchange-correlation function with Grimme-06 semiempirical dispersion correction[54]) using CASTEP.[55] In the calculations, all atom positions and cell parameters were optimized (1200 eV cutoff level).

DOI: 10.1021/jacs.6b09633
J. Am. Chem. Soc. 2016, 138, 15066−15077

Enol-(S)-1. To compare the *trans*-keto and enol structures in detail, the crystal structure of enol-(*S*)-**1** was also optimized, starting from the observed crystal structure,[25] using the same method as for the *trans*-keto-(*S*)-**1** crystal calculations.

Observation of Photomechanical Motion. Thin, platelike enol-(*S*)-**1** crystals were prepared as described above and fixed to the tops of needles. Photomechanical motions upon UV-light irradiation were observed with a digital high-speed microscope (VHX-5000; Keyence). Irradiation was performed by using a UV-LED illuminator (UV-400, 365 nm, 50 mW; Keyence).

Measurement of Linearly Polarized UV−Vis Absorption Spectra of Thin Single Crystals. Enol-(*S*)-**1** crystals prepared by sublimation were fixed on a Cu plate with a pinhole of diameter approximately 0.5 mm. This sample was set on the sample stage of HAUP (Figure S2). The HAUP apparatus is described in the Supporting Information. The spectra of transmitted light intensity at four angles of linearly polarized light in the range of 0−90° (from parallel to perpendicular to the *a* axis) were measured using the HAUP apparatus without analyzer. Then, the spectra of transmitted light intensity were measured under UV light irradiation (10 mW cm^{-2}). After removing enol-(*S*)-**1** crystal, the spectra of transmitted light intensity were measured with and without UV irradiation, as a blank. All measurements were performed at 298 K. Finally, linearly polarized UV−vis absorption spectra were calculated according to the Beer−Lambert−Bouguer law (Figure 5).

Simultaneous Measurement of LB, LD, CB, and CD by HAUP. Enol-(*S*)-**1** and enol-(*R*)-**1** crystals prepared as described above were fixed with silicon grease to a Cu plate with a pinhole of diameter approximately 0.5 mm. This sample was set on the sample stage of HAUP. The HAUP apparatus (Figure S2), theory, and analysis are described in the Supporting Information. HAUP measurements were performed before and under continuous UV irradiation. In the latter case, UV-LED light (365 nm) was continuously irradiated at low power (5 mW cm^{-2}) from a direction almost vertical to the light path of the HAUP to prevent incidence to the photomultiplier tube (Figure S5).

Transition Dipole Moment Calculation. All calculations were carried out with the Gaussian 09 package.[56] We decided to adopt the B3LYP functional[57,58] because it is well-known that hybrid functionals describe the ground and excited state. The 6-311G basis set[59] was applied in conjunction with the B3LYP functional, since it represents a good balance between quality of the results and computational cost. The input molecular geometries of enol-(*S*)-**1** and *trans*-keto-(*S*)-**1** were generated from the calculated crystal structures (Tables S1 and S2). The obtained HOMO and LUMO orbitals of enol-(*S*)-**1** and *trans*-keto-(*S*)-**1** are shown in Figure S10.

Solution CD and ORD Spectrophotometry. Solutions of enol-(*S*)-**1** and enol-(*R*)-**1** in hexane were prepared at the same concentration (500 μM). CD spectra were measured on a circular dichroism spectrometer (J-820; JASCO) with ORD measurement unit (ORD-M) using a standard cell. The scan speed was 200 nm min^{-1}. The cumulated number was 2. The CD, ORD, and absorbance units were converted into molar CD, specific optical rotation, and molar absorption coefficient, respectively.

Calculation of CD Spectra of Various Forms of (*S*)-1. Details of the CD calculation have been described elsewhere.[47] Briefly, all CD calculations were performed on Linux PCs using the Turbomole 6.6 program suite.[60] Geometries were fully optimized at the dispersion-corrected density functional theory (third generation; DFT-D3 with BJ dumping), with an AO basis set of valence triple-ξ quality at the TPSS-D3/def2-TZVP level.[45] The resolution of identity (RI) approximation was employed, and the corresponding auxiliary basis sets were taken from the Turbomole basis set library. The numerical quadrature grid m5 was employed, and the convergence criterion for the optimization regarding the change of total energy between two subsequent optimization cycles was set to 10^{-7} E_h. All excited-state calculations were performed with the above DFT-D3 optimized ground-state geometries, thus corresponding to the vertical transition approximation. The CD spectra were calculated by the time-dependent, second-order approximate coupled-cluster singles and doubles model (RI-CC2 method), employing the same def2-TZVP basis set.[46] A relatively robust length-gauge oscillator strength was used throughout this study. The CD spectra were simulated by overlapping Gaussian functions for each transition, where the width of the band at 1/e height was fixed at 0.4 eV and the overall excitation energy was shifted by 0.3 eV. These values are purely empirical and have no rigorous ground but are able to successfully reproduce and match the experimental CD spectra, thus facilitating interpretation of the spectra.

■ ASSOCIATED CONTENT

Supporting Information

The Supporting Information is available free of charge on the ACS Publications website at DOI: 10.1021/jacs.6b09633.

Detailed HAUP analysis and supporting results (PDF)
CIF by calculation for enol-(*S*)-**1** (CIF)
CIF by calculation for *trans*-keto-(*S*)-**1** (CIF)
Movie S1: bending with twisting motion of a wide and thin platelike microcrystal of enol-(*S*)-1 (354 μm long × 87 μm wide × 10 μm thick) when the (00$\bar{1}$) face was irradiated by UV light. (AVI)
Movie S2: bending with twisting motion of a wide and thin platelike microcrystal of enol-(*S*)-1 (354 μm long × 87 μm wide × 10 μm thick) when the (001) face was irradiated by UV light. (AVI)
Movie S3: bending behavior of a platelike enol-(*S*)-1 crystal (4516 μm long × 380 μm wide × 97 μm thick) when the (00$\bar{1}$) face was irradiated by linearly polarized UV light whose vibration axis is parallel to the *a* axis. (AVI)
Movie S4: bending behavior of a platelike enol-(*S*)-1 crystal (4516 μm long × 380 μm wide × 97 μm thick) when the (00$\bar{1}$) face was irradiated by linearly polarized UV light whose vibration axis is perpendicular to the *a* axis. (AVI)

■ AUTHOR INFORMATION

Corresponding Authors

*E-mail: hkoshima@aoni.waseda.jp.
*E-mail: tasahi@waseda.jp.

Notes

The authors declare no competing financial interest.

■ ACKNOWLEDGMENTS

This work was supported by the JSPS Scientific Research in the Challenging Exploratory Research, and the grant-in-aid from Mitsubishi Materials Corporation. A.T. acknowledges the Leading Graduate Program in Science and Engineering, Waseda University from MEXT, Japan.

■ REFERENCES

(1) Kobatake, S.; Takami, S.; Muto, H.; Ishikawa, T.; Irie, M. *Nature* **2007**, *446*, 778−781.
(2) (a) Al-Kaysi, R. O.; Mueller, A. M.; Bardeen, C. J. *J. Am. Chem. Soc.* **2006**, *128*, 15938−15939. (b) Al-Kaysi, R. O.; Bardeen, C. J. *Adv. Mater.* **2007**, *19*, 1276−1280.
(3) (a) Kuroki, L.; Takami, S.; Yoza, K.; Morimoto, M.; Irie, M. *Photochem. Photobiol. Sci.* **2010**, *9*, 221−225. (b) Morimoto, M.; Irie, M. *J. Am. Chem. Soc.* **2010**, *132*, 14172−14178. (c) Terao, F.; Morimoto, M.; Irie, M. *Angew. Chem., Int. Ed.* **2012**, *51*, 901−904.
(4) Uchida, K.; Sukata, S.; Matsuzawa, Y.; Akazawa, M.; de Jong, J. J. D.; Katsonis, N.; Kojima, Y.; Nakamura, S.; Areephong, J.; Meetsma, A.; Feringa, B. L. *Chem. Commun.* **2008**, *3*, 326−328.
(5) (a) Kobatake, S.; Hasegawa, H.; Miyamura, K. *Cryst. Growth Des.* **2011**, *11*, 1223−1229. (b) Kitagawa, D.; Nishi, H.; Kobatake, S.

DOI: 10.1021/jacs.6b09633
J. Am. Chem. Soc. 2016, 138, 15066−15077

Angew. Chem., Int. Ed. **2013**, *52*, 9320−9322. (c) Kitagawa, D.; Kobatake, S. *J. Phys. Chem. C* **2013**, *117*, 20887−20892. (d) Kitagawa, D.; Kobatake, S. *Photochem. Photobiol. Sci.* **2014**, *13*, 764−769.
(6) (a) Zhu, L.; Agarwal, A.; Lai, J.; Al-Kaysi, R. O.; Tham, F. S.; Ghaddar, T.; Mueller, L.; Bardeen, C. J. *J. Mater. Chem.* **2011**, *21*, 6258−6268. (b) Zhu, L.; Al-Kaysi, R. O.; Bardeen, C. J. *J. Am. Chem. Soc.* **2011**, *133*, 12569−12575.
(7) Kim, T.; Al-Muhanna, M. K.; Al-Suwaidan, S. D.; Al-Kaysi, R. O.; Bardeen, C. J. *Angew. Chem., Int. Ed.* **2013**, *52*, 6889−6893.
(8) Koshima, H.; Uchimoto, H.; Taniguchi, T.; Nakamura, J.; Asahi, T.; Asahi, T. *CrystEngComm* **2016**, *18*, 7305−7310.
(9) (a) Koshima, H.; Ojima, N.; Uchimoto, H. *J. Am. Chem. Soc.* **2009**, *131*, 6890−6891. (b) Koshima, H.; Ojima, N. *Dyes Pigm.* **2012**, *92*, 798−801.
(10) (a) Bushuyev, O. S.; Singleton, T. A.; Barrett, C. *Adv. Mater.* **2013**, *25*, 1796−8000. (b) Bushuyev, O. S.; Tomberg, A.; Friščić, T.; Barrett, C. J. *J. Am. Chem. Soc.* **2013**, *135*, 12556−12559. (c) Bushuyev, O. S.; Corkery, T. C.; Barrett, C. J.; Friščić, T. *Chem. Sci.* **2014**, *5*, 3158−3164.
(11) Koshima, H.; Nakaya, H.; Uchimoto, H.; Ojima, N. *Chem. Lett.* **2012**, *41*, 107−109.
(12) Koshima, H.; Takechi, K.; Uchimoto, H.; Shiro, M.; Hashizume, D. *Chem. Commun.* **2011**, *47*, 11423−11425.
(13) Kim, T.; Zhu, L.; Mueller, L. J.; Bardeen, C. J. *CrystEngComm* **2012**, *14*, 7792−7799.
(14) Naumov, P.; Kowalik, J.; Solntsev, K. M.; Baldridge, A.; Moon, J.-S.; Kranz, C.; Tolbert, L. M. *J. Am. Chem. Soc.* **2010**, *132*, 5845−5857.
(15) Sun, J.-K.; Li, W.; Chen, C.; Ren, C.-X.; Pan, D.-M.; Zhang, J. *Angew. Chem., Int. Ed.* **2013**, *52*, 6653−6657.
(16) Matsunaga, Y.; Goto, K.; Kubono, K.; Sako, K.; Shinmyozu, T. *Chem. - Eur. J.* **2014**, *20*, 7309−7316.
(17) Irie, M.; Fukaminato, T.; Matsuda, K.; Kobatake, S. *Chem. Rev.* **2014**, *114*, 12174−12277.
(18) Kim, T.; Zhu, L.; Al-Kaysi, R. O.; Bardeen, C. J. *ChemPhysChem* **2014**, *15*, 400−414.
(19) Naumov, P.; Chizhik, S.; Panda, K. M.; Nath, K. N.; Boldyreva, E. *Chem. Rev.* **2015**, *115*, 12440−12490.
(20) Abendroth, J. M.; Bushuyev, O. S.; Weiss, P. S.; Barrett, C. J. *ACS Nano* **2015**, *9*, 7746−7768.
(21) *New Frontiers in Photochromism*; Irie, M., Yokoyama, Y., Seki, T., Eds.; Springer: Heidelberg, 2013; Chapters 1 and 2.
(22) Garcia-Garibay, M. A. *Angew. Chem., Int. Ed.* **2007**, *46*, 8945−8947.
(23) Inoue, Y., Ramamurthy, V., Eds. *Chiral Photochemistry*; Marcel Dekker: New York, 2004; Chapters 11−14.
(24) Taniguchi, T.; Fujisawa, J.; Shiro, M.; Koshima, H.; Asahi, T. *Chem. - Eur. J.* **2016**, *22*, 7950−7958.
(25) Koshima, H.; Matsuo, R.; Matsudomi, M.; Uemura, Y.; Shiro, M. *Cryst. Growth Des.* **2013**, *13*, 4330−4337.
(26) Lowry, T. M. *Optical Rotatory Power*; Dover Publications: New York, 1964.
(27) Nye, J. F. *Physical Properties of Crystals*; Oxford University Express: New York, 1985.
(28) Kobayashi, J.; Uesu, Y. *J. Appl. Crystallogr.* **1983**, *16*, 204−211.
(29) Asahi, T.; Utsumi, H.; Itagaki, Y.; Kagomiya, I.; Kobayashi, Z. *Acta Crystallogr., Sect. A: Found. Crystallogr.* **1996**, *52*, 766−769.
(30) Koshima, H.; Nagano, M.; Asahi, T. *J. Am. Chem. Soc.* **2005**, *127*, 2455−2463.
(31) Kobayashi, J.; Asahi, T.; Sakurai, M.; Takahashi, M.; Okubo, K.; Enomoto, Y. *Phys. Rev. B: Condens. Matter Mater. Phys.* **1996**, *53*, 11784−11790.
(32) Tanaka, M.; Nakamura, N.; Koshima, H.; Asahi, T. *J. Phys. D: Appl. Phys.* **2012**, *45*, 175303.
(33) Nakagawa, K.; Harper-Lovelady, H.; Tanaka, Y.; Tanaka, M.; Yamato, M.; Asahi, T. *Chem. Commun.* **2014**, *50*, 15086−15089.
(34) Smith, H. E.; Cook, S. L.; Warren, M. E., Jr. *J. Org. Chem.* **1964**, *29*, 2265−2272.
(35) Heinert, D.; Martell, A. E. *J. Am. Chem. Soc.* **1963**, *85*, 183−188.
(36) (a) Smith, H. E.; Records, R. *Tetrahedron* **1966**, *22*, 813−824. (b) Smith, H. E.; Neergaard, J. R.; Burrows, E. P.; Chen, F. *J. Am. Chem. Soc.* **1974**, *96*, 2908−2916.
(37) Presti, D.; Labat, F.; Pedone, A.; Frisch, M. J.; Hratchian, H. P.; Ciofini, I.; Menziani, M. C.; Adamo, C. *J. Chem. Theory Comput.* **2014**, *10*, 5577−5585.
(38) Toll, J. S. *Phys. Rev.* **1956**, *104*, 1760−1770.
(39) Shen, M. Y.; Zhao, L. Z.; Goto, T.; Mordzinski, A. *J. Chem. Phys.* **2000**, *112*, 2490−2497.
(40) Shopa, Y.; Ftomyn, N. *Acta Phys. Pol., A* **2010**, *117*, 114−116.
(41) Asahi, T.; Nakamura, M.; Kobayashi, J.; Toda, F.; Miyamoto, H. *J. Am. Chem. Soc.* **1997**, *119*, 3665−3669.
(42) Asahi, T.; Takahashi, M.; Kobayashi, J. *Acta Crystallogr., Sect. A: Found. Crystallogr.* **1997**, *53*, 763−771.
(43) Kobayashi, J.; Uchino, K.; Asahi, T. *Phys. Rev. B: Condens. Matter Mater. Phys.* **1991**, *43*, 5706−5712.
(44) Kobayashi, J.; Asahi, T.; Sakurai, M.; Kagomiya, I.; Asai, H.; Asami, H. *Acta Crystallogr., Sect. A: Found. Crystallogr.* **1998**, *54*, 581−590.
(45) (a) Grimme, S.; Antony, J.; Ehrlich, S.; Krieg, H. *J. Chem. Phys.* **2010**, *132*, 154104. (b) Grimme, S.; Ehrlich, S.; Goerigk, L. *J. Comput. Chem.* **2011**, *32*, 1456−1465. (c) Tao, J.; Perdew, J. P.; Staroverov, V. N.; Scuseria, G. E. *Phys. Rev. Lett.* **2003**, *91*, 146401.
(46) (a) Christiansen, R.; Koch, H.; Jørgensen, P. *Chem. Phys. Lett.* **1995**, *243*, 409−418. (b) Hättig, C.; Weigend, F. *J. Chem. Phys.* **2000**, *113*, 5154−5161. (c) Hättig, C.; Kohn, A. *J. Chem. Phys.* **2002**, *117*, 6939−6951.
(47) (a) Wakai, A.; Fukasawa, H.; Yang, C.; Mori, T.; Inoue, Y. *J. Am. Chem. Soc.* **2012**, *134*, 4990−4997. (b) Nakai, Y.; Mori, T.; Sato, K.; Inoue, Y. *J. Phys. Chem. A* **2013**, *117*, 5082−5092. (c) Nakai, Y.; Mori, T.; Inoue, Y. *J. Phys. Chem. A* **2013**, *117*, 83−93. (d) Nakai, Y.; Mori, T.; Inoue, Y. *J. Phys. Chem. A* **2012**, *116*, 7372−7385. (e) Toda, M.; Matsumura, C.; Tsurukawa, M.; Okuno, T.; Nakano, T.; Inoue, Y.; Mori, T. *J. Phys. Chem. A* **2012**, *116*, 9340−9346. (f) Mori, T.; Inoue, Y.; Grimme, S. *J. Phys. Chem. A* **2007**, *111*, 4222−4234. (g) Mori, T.; Grimme, S.; Inoue, Y. *J. Org. Chem.* **2007**, *72*, 6998−7010.
(48) Johmoto, K.; Ishida, T.; Sekine, A.; Uekusa, H.; Ohashi, Y. *Acta Crystallogr., Sect. B: Struct. Sci.* **2012**, *68*, 297−304.
(49) Tanaka, M.; Yagi-Watanabe, K.; Kaneko, F.; Nakagawa, K. *J. Phys. Chem. A* **2010**, *114*, 11928−11932.
(50) Matsuo, K.; Matsushima, Y.; Fukuyama, T.; Senba, S.; Gekko, K. *Chem. Lett.* **2002**, *31*, 826−827.
(51) Goto, T.; Ikehata, A.; Morisawa, Y.; Ozaki, Y. *J. Phys. Chem. A* **2013**, *117*, 2517−2528.
(52) (a) Harada, J.; Ogawa, K.; Tomoda, S. *Acta Crystallogr., Sect. B: Struct. Sci.* **1997**, *53*, 662−672. (b) Harada, J.; Ogawa, K. *Chem. Soc. Rev.* **2009**, *38*, 2244−2252.
(53) (a) Harada, J.; Uekusa, H.; Ohashi, Y. *J. Am. Chem. Soc.* **1999**, *121*, 5809−5810. (b) Johmoto, K.; Sekine, A.; Uekusa, H.; Ohashi, Y. *Bull. Chem. Soc. Jpn.* **2009**, *82*, 50−57.
(54) Marom, N.; Tkatchenko, A.; Rossi, M.; Gobre, V. V.; Hod, O.; Scheffler, M.; Kronik, L. *J. Chem. Theory Comput.* **2011**, *7*, 3944−3961.
(55) Clark, S. J.; Segall, M. D.; Pickard, C. J.; Hasnip, P. J.; Probert, M. J.; Refson, K.; Payne, M. C. *Z. Kristallogr. - Cryst. Mater.* **2005**, *220*, 567−570.
(56) Frisch, M. J.; Trucks, G. W.; Schlegel, H. B.; Scuseria, G. E.; Robb, M. A.; Cheeseman, J. R.; Scalmani, G.; Barone, V.; Mennucci, B.; Petersson, G. A.; Nakatsuji, H.; Caricato, M.; Li, X.; Hratchian, H. P.; Izmaylov, A. F.; Bloino, J.; Zheng, G.; Sonnenberg, J. L.; Hada, M.; Ehara, M.; Toyota, K.; Fukuda, R.; Hasegawa, J.; Ishida, M.; Nakajima, T.; Honda, Y.; Kitao, O.; Nakai, H.; Vreven, T.; Montgomery, J. A., Jr.; Peralta, J. E.; Ogliaro, F.; Bearpark, M.; Heyd, J. J.; Brothers, E.; Kudin, K. N.; Staroverov, V. N.; Kobayashi, R.; Normand, J.; Raghavachari, K.; Rendell, A.; Burant, J. C.; Iyengar, S. S.; Tomasi, J.; Cossi, M.; Rega, N.; Millam, J. M.; Klene, M.; Knox, J. E.; Cross, J. B.; Bakken, V.; Adamo, C.; Jaramillo, J.; Gomperts, R.; Stratmann, R. E.; Yazyev, O.; Austin, A. J.; Cammi, R.; Pomelli, C.; Ochterski, J. W.; Martin, R. L.; Morokuma, K.; Zakrzewski, V. G.; Voth, G. A.; Salvador, P.; Dannenberg, J. J.; Dapprich, S.; Daniels, A. D.; Farkas, O.;

DOI: 10.1021/jacs.6b09633
J. Am. Chem. Soc. 2016, 138, 15066−15077

Foresman, J. B.; Ortiz, J. V.; Cioslowski, J.; Fox, D. J. *Gaussian 09*, revision B.01; Gaussian, Inc.: Wallingford, CT, 2009.
(57) Becke, A. D. *J. Chem. Phys.* **1993**, *98*, 5648−5652.
(58) Lee, C.; Yang, W.; Parr, R. *Phys. Rev. B: Condens. Matter Mater. Phys.* **1988**, *37*, 785−789.
(59) Krishnan, R.; Binkley, J. S.; Seeger, R.; Pople, J. A. *J. Chem. Phys.* **1980**, *72*, 650−654.
(60) *Turbomole*, V6.6 2014; Turbomole GmbH: Karlsruhe, Germany, 2014. http://www.turbomole.com.

DOI: 10.1021/jacs.6b09633
J. Am. Chem. Soc. 2016, 138, 15066−15077